Research Article

Effect of Nanosilica on Impermeability of Cement-Fly Ash System

Huaqing Liu,[1] Yan Zhang,[1] Ruiming Tong,[1] Zhaoqing Zhu,[1] and Yang Lv [2]

[1]*China Electric Power Research Institute, Beijing 100192, China*
[2]*State Key Laboratory of Silicate Materials for Architectures, Wuhan University of Technology, Wuhan 430070, China*

Correspondence should be addressed to Yang Lv; yang.lv@whut.edu.cn

Surface protection has been accepted as an effective way to improve the durability of concrete. In this study, nanosilica (NS) was used to improve the impermeability of cement-fly ash system and this kind of material was expected to be applied as surface protection material (SPM) for concrete. Binders composed of 70% cement and 30% fly ash (FA) were designed and nanosilica (NS, 0–4% of the binder) was added. Pore structure of the paste samples was evaluated by MIP and the fractal dimension of the pore structure was also discussed. Hydrates were investigated by XRD, SEM, and TG; the microstructure of hydrates was analyzed with SEM-EDS. The results showed that in the C-FA-NS system, NS accelerated the whole hydration of the cement-FA system. Cement hydration was accelerated by adding NS, and probably, the pozzolanic reaction of FA was slightly hastened because NS not only consumed calcium hydroxide by the pozzolanic reaction to induce the cement hydration but also acted as nucleation seed to induce the formation of C-S-H gel. NS obviously refined the pore structure, increased the complexity of the pore structure, and improved the microstructure, thereby significantly improving the impermeability of the cement-FA system. This kind of materials would be expected to be used as SPM; the interface performance between SPM and matrix, such as shrinkage and bond strength, and how to cast it onto the surface of matrix should be carefully considered.

1. Introduction

Concrete has been widely employed in civil constructions in the past decades, and the main reason is due to its excellent performance, especially long life serving [1, 2]. However, reinforced-concrete structures inevitably suffer from damages in harsh environment, such as in the presence of chloride ions, carbon dioxide, and sulphate, resulting in shortening its life [3–6]. The generally accepted reason for those is that concrete is a porous material with microstructural defect, and the harmful ions could penetrate the surface into the inside of concrete structure and cause corrosion, finally leading to crack [7, 8]. For example, sulphate was able to penetrate the surface into the inside and react with hydrates to produce ettringite or gypsum, associating with a volume expansion. The mechanical performance could be deteriorated, and under load, the cracks occurred; thereafter, sulphate ions were easier to go into the inside of concrete structure along the cracks and the more serious corrosion would happen [9–11]. Chloride ions could easily permeate into the inside of the matrix and migrate to

the surface of steels and then cause steel corrosion probably [12, 13]; finally, volume expansion happened and the concrete structure was destroyed. In the process of various external erosions, one precondition is that corrosion ions need to penetrate through the surface and go into the inside of the concrete. Accordingly, surface protection has been accepted as one of the most popular way to promote the concrete durability in actual engineering process [14].

Coating a film on the surface of concrete is one of the main methods for surface protection [15]. Two kinds of surface protection materials (SPM) were reported in the literature. One was the penetrative protective agent based on organic materials, with intention to block the surface pore structure; the other was the inorganic materials, such as mortar or cement paste, to isolate the matrix from erosion ions in outside environment. Silanes [16], ethyl silicate [17, 18], and isobutyl-triethoxy-silane [19] were used as typical penetrative protective agents for the resistance of carbonation and erosion, and a silica-based hybrid nanocomposite was reported for surface treatment to reduce the water absorption and gas permeability [20]. One mechanism

behind the enhanced impermeability was that the chemicals could go through the capillary and form an inorganic hydrophobic film along the capillary as a result of reacting with hydration products; the other was that these hydrates in the capillary structure would block the transportation of water and gas [21]. Furthermore, another kind of SPM was coated as a layer on the surface of the matrix. Zhang reported that cement mortar modified with nanosilica (NS) and silica fume could be used as SPM to enhance the impermeability [22]. The reason was revealed that NS and silica fume not only consumed CH to form the dense C-S-H but also exerted the excellent filling effect, thereby declining the porosity, increasing density, improving the microstructure including interfacial transition zone (ITZ), and enhancing the mechanical performance [23–26]. Additionally, the inorganic materials generally performed better antiaging property and also showed excellent ability to augment the impermeability by coating on the surface [27, 28].

In the literature, incorporating mineral admixtures, such as fly ash and ground granulated blast furnace slag (GGBS), could not only exhibit economic and environmental benefits [29–31] but also greatly improve the durability of cementitious materials [32, 33]. In this paper, the cement-fly ash-NS system was designed and used as a SPM. 30% fly ash (FA) and NS (0–4%) were added with the intention to improve the impermeability. The chloride diffusion coefficient of SPM was determined to illustrate the effect of NS addition on the impermeability of SPM under investigation. Furthermore, the properties of the pore structure, microstructure, and hydration products of SPM were investigated to reveal the mechanism of its high impermeability. The pore structure was discussed by compressive strength, water absorption, and MIP; microstructure was investigated with SEM-EDS. Hydrates were evaluated with XRD, TG-DSC, NMR, and SEM. The findings would expect to be useful for the design of surface protection materials.

2. Experimental

2.1. Materials

2.1.1. Cement and Fly Ash. A 42.5 Portland cement (Wuhan Yadong Cement Co., Ltd.) in accordance with the requirements of GB175-2007 Chinese standard and coal-fired fly ash (produced by Wuhan Yangluo Power Plant, Wuhan, Hubei province) in accordance with the requirements of GB/T 1596–2005 Chinese standard were used in this study. The chemical composition of cement and fly ash (obtained by XRF) are shown in Table 1. Particle size distribution and SEM image of FA are shown in Figures 1(a) and 1(b).

2.1.2. Nanosilica. The average particle diameter of powdered nanosilica (NS, supplied by Sinopharm Chemical Reagent Co., Ltd.) used in this study was about 15–20 nm, which was indicated from the TEM image, as shown in Figure 2.

2.1.3. Preparation of Samples. The mortar samples were prepared according to the mixture proportion, as shown in

Table 2. Because NS showed negative effect on the workability of C-FA system [34], the same fluidity level (160–180 mm) was controlled by adding PCE. NO.0 mortar was deemed as the reference sample. Cement and fly ash was firstly mixed, and then the NS suspension, dispersed by PCE [35] and water, was added. After that, sand was added within 30 s, followed by continuous stirring for 90 s, and then SPM was prepared. After the samples were cured in the standard condition (>95% R.H. and 20 ± 1°C) for 24 h, they were demoulded and further cured till 28 d. These mortars were also cast in the model with ϕ100 mm and 50 mm height and cured under the same condition till 28 d. In accordance with Chinese standard GB/T 50082-2009, rapid chloride migration (RCM) was used for the measurement of chloride diffusion coefficient. The sand used in experiments was Standard Sands (GSB 08-1337-2017, supplied by Xiamen aisio standard sand Co., Ltd.).

These fresh mortars were also cast in the cubic moulds (40 × 40 × 40 mm). After being cured for 7 d, 28 d, and 90 d under standard condition, the measurements of compressive strength, water absorption, and microstructure were conducted.

The cement pastes were also prepared, as shown in Table 2, and cured under the standard condition for 28 d. The samples were broken into small pieces and immersed into the anhydrous ethanol for 48 h to stop its hydration. These small pieces were prepared for the measurement of SEM and pore structure. Furthermore, the broken pieces were grinded into powder to pass a 45 μm sieve, being ready for the analysis of XRD, TG, and NMR.

2.2. Testing Methods

2.2.1. Chloride Penetrability. Mortar samples were put into a vacuum container for 3 hours, followed by being immersed into saturated Ca(OH)$_2$ solution for 18 ± 2 h. 0.3 mol/L NaOH and 10 wt% NaCl were used as cathode solution and anode solution. External electrical potential (30 ± 0.2 V) was employed to the upper and lower section of the samples. After the measurement, the samples were carefully cleaned and then split into two semicylinders along the axial direction. Finally, 0.1 mol/L silver nitrate solution was sprayed on the cross section, and the chloride penetration depth of the specimen was measured at 10 different locations. Three samples were used for each test group. The D_{RCM} was calculated as follows:

$$D_{RCM} = \frac{0.0239 \times (273 + T)L}{(U - 2)t}\left(X_d - 0.0238\sqrt{\frac{(273 + T)LX_d}{U - 2}}\right),$$

$$(1)$$

where D_{RCM} denoted the chloride diffusion coefficient, m^2/s; U reflected the applied voltage, V; T represented the average temperature of anode solution, °C; L denoted the height of sample, mm; X_d showed the chloride ion penetration depth, mm; and t indicated the test time, h.

2.2.2. Compressive Strength. The compressive strength of mortars was conducted under a loading rate was 2.4 kN/s, in agreement with Chinese standard (GB/T17671-1999). For each age, three specimens were tested to obtain the average result.

TABLE 1: Chemical composition of cement and fly ash/wt.%.

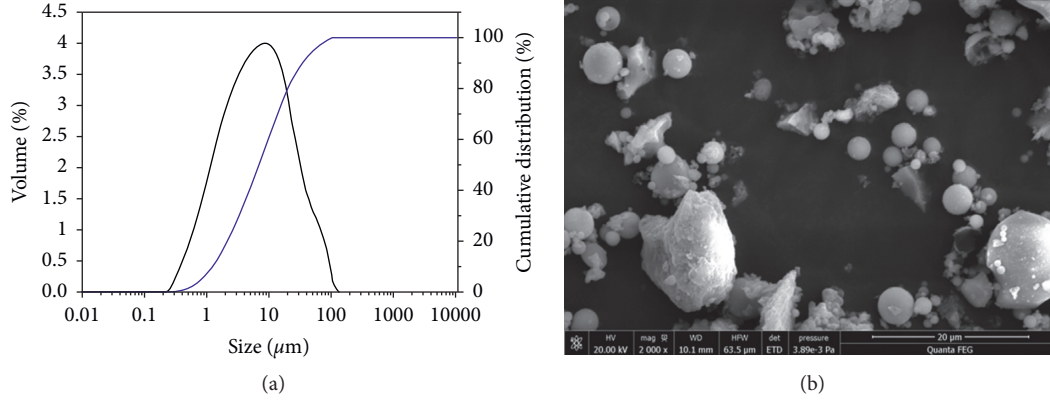|	LOI	SiO$_2$	Al$_2$O$_3$	Fe$_2$O$_3$	SO$_3$	CaO	MgO	K$_2$O	Na$_2$O
Cement	3.56	22.18	5.88	3.57	2.00	59.41	1.80	0.64	0.13
Fly ash	6.53	55.31	28.63	3.65	0.68	3.80	0.43	0.13	0.76

(a)

(b)

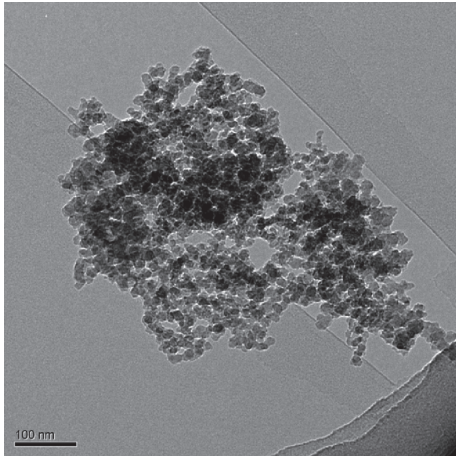FIGURE 1: (a) Particle size distribution and (b) SEM image of FA.

FIGURE 2: TEM image of nanosilica.

2.2.3. Water Absorption. The water absorption of cement mortars cured for 28 d was tested according to GB/T 17671. The specimen was dried in an oven with temperature of $80 \pm 2°$C for 48 h and then removed and cooled to room temperature. After that the mass of the sample (G_0) was weighted and then immersed into water with the temperature of 20 ± 2 °C for 48 h; thereafter, the sample was taken out of the water, and the water on the surface was cleaned; the mass of the sample (G_1) was weighted again. Water absorption (equation (2)) was calculated as follows:

$$W_A = \frac{G_1 - G_0}{G_0} \times 100\%, \qquad (2)$$

where W_A, water absorption (%); G_0, the mass of the specimen after drying (g); and G_1, the mass of the specimen after adsorbing water (g).

2.2.4. Phase Analysis. The measurement of XRD was conducted with X-ray Diffractometer (D/Max-RB, made by Rigaku, Japan) with Cu (Kα) radiation and a current of 40 mA at 40 kV, at a speed of 2θ 4°/min and a step of 0.02° within the range from 5 to 70°. The data was processed with Jade 5.0.

The measurement of TG-DSC was carried out with the instrument of STA449c/3/G (NETZSCH, Germany) under an atmosphere of flowing air from room temperature to 1000°C at a heating rate of 10°C/min. The accurate content of calcium hydroxide (CH) was calculated from the weight loss ranging from 400–500°C [36, 37].

Morphology characterization of hydrates in the paste sample was conducted with Field Emission Scanning Electron Microscope (FE-SEM, QUANTA FEG 450).

2.2.5. NMR. The hydration products were characterized with ^{29}Si MAS NMR. It was reported that six peaks were found in NMR spectrum of hydrated cement-FA paste [12, 38, 39]; Q^1 and Q^2 represented the chain-end Si-O tetrahedrons and middle-chain Si-O tetrahedrons in hydration products; Q^2(1Al) denoted the middle-chain groups where one of the adjacent tetrahedral sites was occupied by Al^{4+}; Q^0, Q^3, and Q^4 represented the Si-O tetrahedrons in unhydrated cement minerals and Si-O tetrahedrons in FA, respectively. A Bruker Advance III400 spectrometer was adopted to carry out ^{29}Si-NMR (solid-state nuclear magnetic resonance), operating at 79.5 MHz, with rotation frequency of 5 kHz and the delay time of 10 s. Tetramethylsilane was used as ^{29}Si standard. The data were processed with commercial solid-state NMR software package. During the deconvolution of ^{29}Si NMR spectra, the peak was fitted and Gaussian function was used to constrain the peak shapes. The main chain length (MCL, equation (3)) of C-S-H gel and the ratio of Si in C-S-H substituted by Al (equation (4)) were obtained as follows [40–42]:

TABLE 2: Mix proportion of mortars and paste.

NO.	NS (%)	NS (g)	Cement (g)	FA (g)	Sand (g)	Water (g)	PCE (g)
0	0	0	350	135	1350	225	0
1	0.5	2.25	347.75	135	1350	225	0.5
2	1.0	4.50	345.5	135	1350	225	1
3	1.5	6.75	343.25	135	1350	225	1.3
4	2.0	9.00	341	135	1350	225	1.5
5	4.0	18.00	332	135	1350	225	1.8

$$\text{MCL} = \frac{2I(Q^1) + 2I(Q^2) + 3I[Q^2(\text{Al})]}{I(Q^1)}, \tag{3}$$

$$\frac{\text{Al}}{\text{Si}} = \frac{0.5I[Q^2(\text{Al})]}{I(Q^1) + I(Q^2) + I[Q^2(\text{Al})]}. \tag{4}$$

Reaction degree of cement is shown in equation (5). Reaction degree of FA in the C-FA system is exhibited in equation (6). Because Q^3 and Q^4 are also presented in NS, it is difficult to calculate the hydration degree of FA and NS, respectively. However, the total reaction degree of FA and NS could be calculated, as shown in equation (7). It was reported that most of NS was depleted at the early age [43]. Based on this, $A_{(\text{FA}+\text{NS})}$ could reflect the pozzolanic reaction of FA:

$$A_C(\%) = 1 - \frac{I(Q^0)}{I_0(Q^0)}, \tag{5}$$

$$A_{\text{FA}}(\%) = 1 - \frac{I(Q^3 + Q^4)}{I_0(Q^3 + Q^4)}, \tag{6}$$

$$A_{(\text{FA}+\text{NS})}(\%) = 1 - \frac{I(Q^3 + Q^4)}{I_0(Q^3 + Q^4)}, \tag{7}$$

where $I(Q^0)$, $I(Q^1)$, $I(Q^2)$, and $I[Q^2(\text{Al})]$ denoted the intensities of signals Q^0, Q^1, Q^2, and $Q^2(\text{Al})$ in hydrated paste, respectively; $I_0(Q^0)$, $I_0(Q^3)$, and $I_0(Q^4)$ represented the intensities of signals Q^0, Q^3, and Q^4 in unhydrated mixture.

2.2.6. Pore Structure. Mercury intrusion porosimetry (Auto Pore IV 9510, America) was used for pore structure characterization. The calculation of pore distribution assumes that the pores are spherical in shape, with the surface tension of mercury of 480 mN/m and contact angle of 140°.

During the measurement of MIP, external pressure on mercury was equal to the surface energy increased by pores and the correlation appeared in

$$dW = -PdV = -\gamma_L \cos\theta \, dS, \tag{8}$$

where W is the surface energy of the pore; P is the mercury pressure; V is the intruded mercury volume; γ_L is the surface tension of mercury; θ is the contact angle of mercury with the surface of the pore; and S is the surface area of the pore.

In the literature, the relationship between the accumulated intrusion surface energy (W_n) and the accumulated mercury intrusion surface (Q_n) (shown in equation (9)) was proposed by Zhang and Li [44]. Based on this, the accumulated mercury volume is V_n and the smallest pore radius is r_n; then, W_n and Q_n are expressed as equations (10) and (11):

$$\log W_n = \log Q_n + C, \tag{9}$$

$$W_n = \sum_{i=1}^{n} P_i \Delta V_i, \tag{10}$$

$$Q_n = r_n^{2-D} V_n^{3/D}, \tag{11}$$

where C is a constant; P_i and V_i stand for the mercury pressure and intruded pore volume at step i; and D stands for the fractal dimension of the pore surface [45–48].

Therefore, equation (9) is expressed as equation (12). The fractal dimension of the pore surface can be obtained by the slope of the curve $\log(V_n^{1/3}/r_n)$ versus $\log(W_n/r_n^2)$. Greater than 0.99 was controlled in the correlation coefficient:

$$\log\left(\frac{W_n}{r_n^2}\right) = D \log\left(\frac{V_n^{3/D}}{r_n}\right) + C. \tag{12}$$

2.2.7. Analysis of Microstructure. The mortar samples were dried under vacuum and coated with a golden film, and then, a scanning electron microscope (SEM-EDS, JSM-5610LV, Japan) equipped with an energy dispersive spectrometer (EDS, made by EDAX Inc., USA) was employed to observe the microstructure. Based on EDS, different phases were reflected from different colors, and the element content (C) in each phase and the ratio of each phase (A) in the whole image was read directly from the EDS data. Based on these results, the average Ca/Si ratio (equation (13)) and the Ca/Si ratio of each phase (equation (14)) were calculated as follows [49]:

$$\frac{\text{Ca}}{\text{Si}} \text{ in } n\text{phase} = \frac{C_{n-\text{Ca}}}{C_{n-\text{Si}}}, \tag{13}$$

$$\text{Average } \frac{\text{Ca}}{\text{Si}} \text{ in whole image} = \frac{\sum(C_{n-\text{Ca}} \times A_n)}{\sum(C_{n-\text{Si}} \times A_n)}, \tag{14}$$

where $C_{n-\text{Ca}}$ and $C_{n-\text{Si}}$ mean Ca and Si content in n phase, and this phase occupied A_n ratio in this SEM image.

3. Results and Discussion

3.1. Chloride Penetrability. Chloride diffusion coefficient (D_{RCM}) of the C-FA-NS system was examined, and the results are shown in Figure 3. From the figure, it was seen
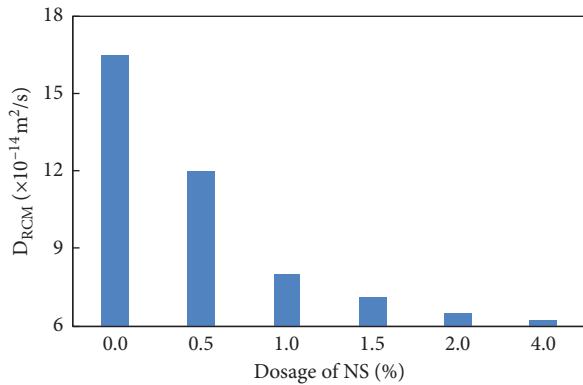
FIGURE 3: Effect of NS on chloride diffusion coefficient of the C-FA-NS system.

FIGURE 4: Effect of NS on water absorption of the C-FA system.

that D_{RCM} was declined obviously with increasing dosage of NS. In the absence of NS, the value was about 16.5×10^{-14} m²/s, while 0.5% NS reduced it to 12×10^{-14} m²/ s; increase in dosage to 4.0% further reduced it to 6.2×10^{-14} m²/s. These results illustrated that addition of NS into the cement-FA system significantly increased the impermeability of the system. This is consistent with the result in the literature [8, 22].

It is generally believed that the impermeability of cement-based material is related to the pore structure and microstructure [50]. Improvement in the microstructure and refining of the pore structure would significantly augment the impermeability. These would be further discussed in the following text.

3.2. Pore Structure.
The pore structure was investigated in terms of water absorption, MIP, and compressive strength and shown as follows.

3.2.1. Water Absorption of C-FA-NS System.
Water absorption of the C-FA system with various dosages of NS cured for 28 d are shown in Figure 4. It can be seen that the water absorption was reduced with the increasing dosage of NS. Addition of 0.5% NS reduced the water absorption by 5.45% and increase in dosage to 4.0% further reduced it by 21.82%, in comparison with the reference (without NS). As reported in the literature [51, 52], water absorption reflected the surface pore structure of the mortar. Generally, greater water absorption represented more amount of open pore which was related to the impermeability. Based on this, it was inferred that NS in the C-FA system significantly improved the surface pore structure, which was responsible for the enhanced impermeability.

3.2.2. MIP.
The pore structure was characterized with MIP, and the results are shown in Figure 5 and Table 3. From the figure, it was seen that addition of NS could obviously refine the pore structure of the C-FA system, and the most probable aperture (MPA) was notably reduced by adding NS, in agreement with the results in the literature [53, 54]. In Table 3, it was found that NS reduced the porosity of C-FA
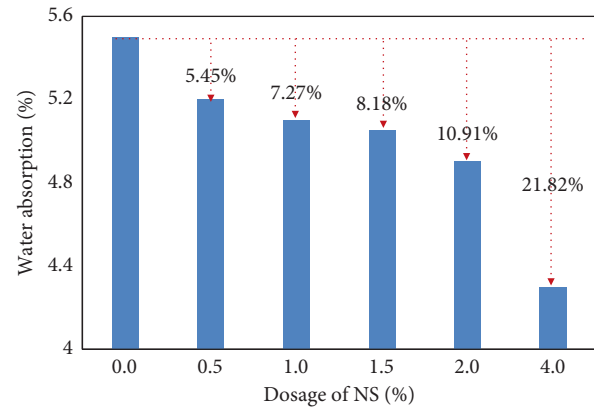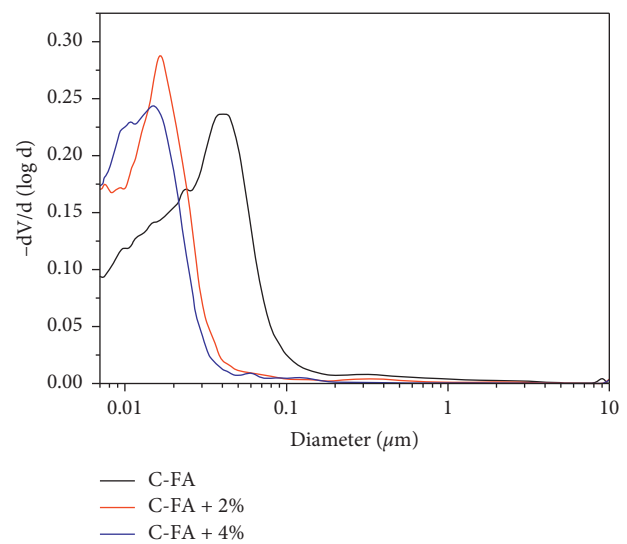

FIGURE 5: Pore size distribution of C-FA with NS.

from 0.1808 mL/g in reference (C-FA) to 0.1448 mL/g and 0.1304 mL/g in sample with 2.0% NS and 4.0% NS, respectively. Additionally, NS notably increased the pore volume with size smaller than 20 nm, while significantly reducing the pore volume with size bigger than 200 nm. These results implied that NS, with nanoscale particles, was able to significantly refine the pore structure [55–57]. Similar results concerning nanoparticles were also reported in the literature [58–62].

The microporous structure was related to transport properties of cement paste, which could be reflected by fractal dimension. In this study, fractal characteristics of the pore structure was calculated from MIP data [45, 48, 63], and the results are posted in Figure 6. It was observed that two fractal areas were separated by a transition area. It was reported that Ds-a of the macrofractal region represented the packing patterns of the hydrated binder particles, while the Ds-i of the differential region mainly showed the microstructure of the C-S-H gel [45, 46]. 2% and 4% NS increased the Ds-a of the samples from 2.006 in reference to 2.066 and 2.329 and increased Ds-i from 2.685 in reference

TABLE 3: Pore structure of C-FA with NS.

Sample	Porosity (mL/g)	Pore volume distribution (mL/g)			
		<20 nm	20~50 nm	50~200 nm	>200 nm
C-FA	0.1808	0.0563	0.0795	0.0332	0.0118
C-FA + 2%	0.1448	0.0961	0.0357	0.0029	0.0101
C-FA + 4%	0.1304	0.0994	0.0225	0.0026	0.0059
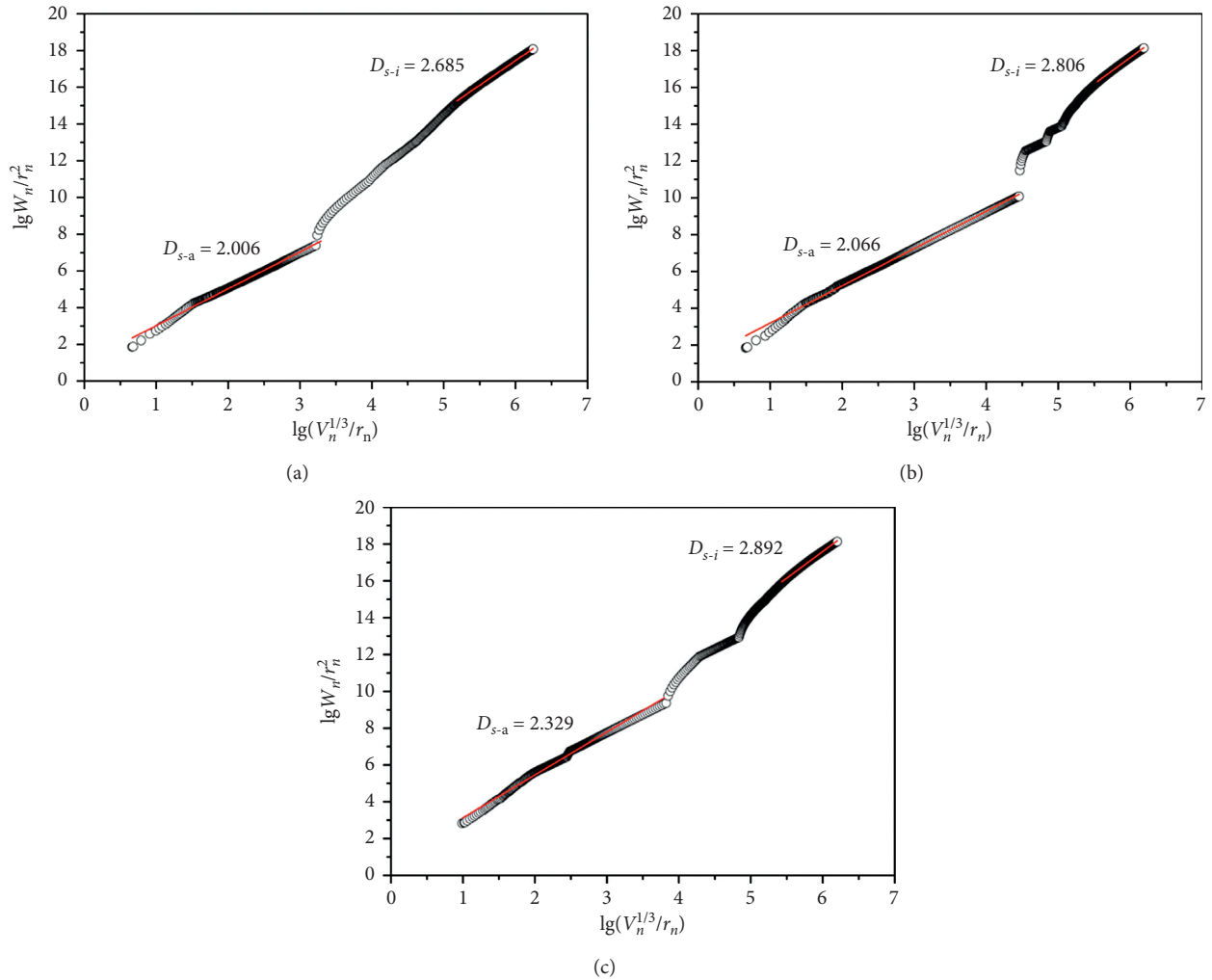
FIGURE 6: Logarithm plots of W_n/r_n^2 versus $V_n^{1/3}/r_n$ of the C-FA system with NS. (a) C-FA. (b) C + FA + 2%. (c) C + FA + 4%.

to 2.806 and 2.892. These phenomena indicated that the addition of NS disordered the transport tunnel and made the pore structure more tortuous at the age of 28 d, which could reduce the transport properties of the hardened paste.

3.2.3. Compressive Strength. Compressive strength was used to offer the supplementary evidence to illustrate the pore structure [64, 65]. The compressive strength of the C-FA-NS system cured for 7 d, 28 d, and 90 d was examined, and the results are shown in Figure 7. With the increasing dosage of NS, 7 d strength and 28 d strength were increased. Especially at the age of 7 d, 2.0% NS increased the strength from 21.0 MPa in reference to 30 MPa, with an increase by 43%; the increase

rate is by 11% for 28 d, while in the case of 90 d, the NS containing sample showed lower strength than the reference sample. As reported in the literature, the increased strength at the early age was related to the refined pore structure and the accelerated hydration process, while the reduced strength at the later age was due to the coating effect resulting from pozzolanic reaction of NS on the surface of FA [66].

Based on discussion about the water absorption, MIP, and compressive strength, it can be concluded that NS added in the C-FA system could significantly refine the pore structure of the system. With increase in curing age, the hardened structure was densified, showing compacter structure, which was inferred conducive to impermeability of the system [67].
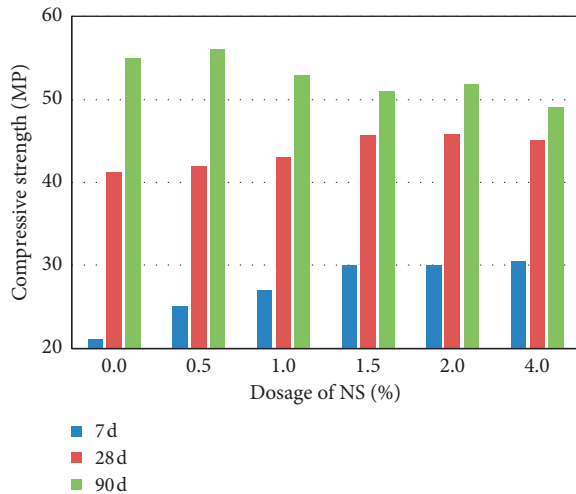
Figure 7: Effect of NS on compressive strength of the C-FA system.

3.3. Microstructure of Hydrates.

Microstructure in ITZ is accepted as one of the main factors influencing the impermeability of the mortar [68]. Generally, the width of ITZ was 20–50 μm. In this section, area 100–150 μm away from aggregate was investigated by SEM-EDS, as shown in Figure 8. From the figure, ITZ was not obviously observed. Furthermore, analysis about the microstructure of these areas was carried out, and Ca, Si, and phase distribution in different phases was displayed in Table 4. It can be found that the Ca/Si ratio of the red color was as low as 0.02, indicating that the red color represented the sand. Furthermore, as shown in Table 4, the average Ca/Si ratio in image was calculated. In the C-FA (reference) system, the average Ca/Si ratio was 1.86; 2.0% NS reduced it to 1.52, and increase in dosage to 4.0% further reduced it to 1.43. In fact, the Ca/Si ratio in hydrates reflected the CH content in C-S-H, and generally, higher Ca/Si ratio meant greater amount of CH. Based on this, the reduced Ca/Si ratio by adding NS could be explained from the fact that NS with nanosize entered these areas near the aggregates and reacted with CH to reduce the Ca/Si ratio. The whole microstructure including the microstructure of ITZ was improved significantly, with obvious contribution to the strength.

3.4. Phase Analysis.

In order to discuss the effect of NS on hydration properties of the C-FA system, the samples were investigated with XRD, TG, and NMR.

3.4.1. XRD.

The peak intensity of CH in the XRD pattern could reflect the relative content of CH in hydrates, which illustrated the hydration process of the cementitious system [69]. In the C-FA-NS system, cement hydration produced CH, and the pozzolanic reaction of FA and NS consumed CH to reduce the amount of CH in hydrates [70]. The paste cured for 28 d was characterized with XRD, and the results are shown in Figure 9. From the figure, CH, ettringite (AFt), C_3S, portlandite, and mullite were seen clearly. It was found that NS significantly reduced the peak intensity of CH and

slightly enhanced the peak intensity of AFt, while obvious change of the peak intensity of C_3S and mullite was not observed. It was confirmed that the reaction between NS and CH happened. It was deduced that the consumption of CH by this reaction could induce cement hydration. Obviously, the consumption of CH by NS was dominated, and therefore, the reduced CH peak intensity by adding NS was observed.

3.4.2. TG-DTG.

To further confirm the content of CH in hydrates, TG-DTG was employed. As shown in Figure 10, the peaks ranging from 50–200°C and 400–500°C were seen clearly. The former represented the dehydration of C-S-H and AFt, and the later denoted the decomposition of CH. Table 5 illustrates the weight loss calculated by TG.

From the table, it was found that NS addition increased the weight loss occurring at 50–200°C. In the C-FA system, the weight loss within the temperature range of 50–200°C was 7.46%; 2.0% NS increased it to 8.29%; increase in dosage to 4.0% further increased it to 9.05%. This result indicated that NS accelerated the formation of hydration products such as AFt or C-S-H gel. Furthermore, the weight loss at 400–500°C was also reduced from 3.21% in C-FA to 2.67% in C-FA-2.0% NS system and 2.04% in C-FA-4.0% NS system. Based on this, the CH content was calculated; in the C-FA system, the CH content was 7.85%, and 2.0% and 4.0% NS reduced it to 6.53% and 4.99%. It was clear that NS reduced the content of CH in hydrates. The results agreed with the results in XRD analysis. The mechanism behind was revealed as follows: NS would react with CH to produce the C-S-H gel, and the consumption of CH would induce the cement hydration to generate more CH. NS with nanoparticles could also act as nucleation seed to induce the hydration of cement to produce hydrates [37, 71, 72]. In this case, cement hydration was hastened in the following age.

3.4.3. NMR.

NMR was used to analyze the hydration products. The NMR pattern obtained from paste hydrated for 28 d are shown in Figure 11. In the process of hydration, Q^0 was due to the unhydrated cement; Q^3 and Q^4 were attributed to unhydrated FA and NS. As shown in Figure 11, the intensity of Q^0, Q^3, and Q^4 in raw materials reduced, while that for Q^1, Q^2, and $Q^2(1Al)$ in hydrates increased obviously, indicating the hydration of cement and FA as well as the formation of C-S-H gel. As shown in Table 6, in the C-FA system, the reaction ratio of cement was 58.68%; 2.0% NS increased the reaction ratio of cement to 64.91%. Furthermore, it was noted that the total reaction degree of FA and NS could be calculated as 14.77%; the reaction degree of FA could not be directly obtained. As the value of $A_{(FA+NS)}$ was 4.74% higher than that of A_{FA}, it is most likely that hydration of FA was slightly promoted in the C-FA-NS system in comparison with C-FA. NS also increased the MCL value from 3.94 in the C-FA system to 4.40 in 2% NS system and 4.48 in 4.0% NS system, indicating that NS accelerated the polycondensation of C-S-H gel in the system. The Al/Si ratio was also increased by addition of NS, indicating that NS accelerated the dissolution of aluminate
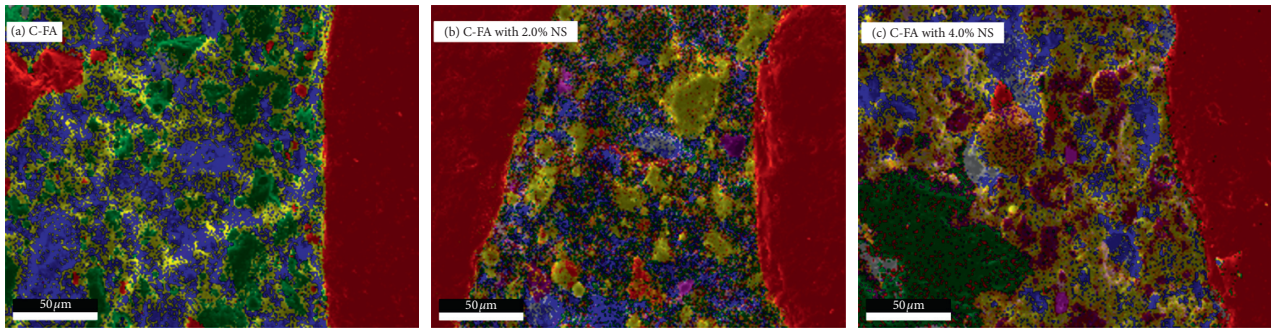
Figure 8: SEM-EDS images of the mortar.

Table 4: Phase distribution in samples.

Sample	Phase	🟥	🟨	🟦	🟩	🟧	🟫	🟪(pink)	⬜	🟪	Average Ca/Si
C-FA	Phase proportion (%)	26.00	28.00	29.00	16.00						
	Ca (%)	0.66	14.72	23.89	6.24						
	Si (%)	36.70	8.98	6.43	13.19						1.86
	Ca/Si	0.02	1.64	3.72	0.47						
	Total Ca (%)	0.17	4.12	6.93	1.00						
	Total Si (%)	9.54	2.51	1.86	2.11						
C-FA with 2% NS	Proportion (%)	39.00	11.00	10.00	12.00	10.00	8.00	6.00	3.00	1.00	
	Ca (%)	0.48	4.11	21.30	15.08	7.06	7.97	11.45	10.06	2.21	
	Si (%)	29.19	9.93	3.74	8.07	11.81	4.43	4.20	5.55	3.76	1.52
	Ca/Si	0.02	0.41	5.70	1.87	0.60	1.80	2.73	1.81	0.59	
	Total Ca (%)	0.19	0.45	2.13	1.81	0.71	0.64	0.69	0.30	0.02	
	Total Si (%)	11.38	1.09	0.37	0.97	1.18	0.35	0.25	0.17	0.04	
C-FA with 4% NS	Proportion (%)	22.00	19.00	14.00	13.00	13.00	4.00	5.00	2.00	8.00	
	Ca (%)	0.54	15.28	28.21	2.24	10.20	5.58	7.32	16.25	4.21	
	Si (%)	35.02	4.66	3.12	21.90	8.72	9.26	3.04	6.84	10.66	1.43
	Ca/Si	0.02	3.28	9.04	0.10	1.17	0.60	2.41	2.38	0.39	
	Total Ca (%)	0.12	2.90	3.95	0.29	1.33	0.22	0.37	0.33	0.34	
	Total Si (%)	7.70	0.89	0.44	2.85	1.13	0.37	0.15	0.14	0.85	

from FA into the liquid phase to take part in formation of C-S-H gel [73–75]. Based on this, it was confirmed that the cement hydration was promoted; and probably, pozzolanic hydration of FA was slightly accelerated by adding NS.

3.4.4. SEM. Microstructure of hydrates at the age of 28 d was characterized by SEM, and the SEM images are shown in Figure 12. From Figure 12(a), C-S-H gel and FA were seen clearly, and a small amount of hydrates on the surface of FA was found. In Figure 12(b), a large amount of hydration products on the surface of FA was found clearly; fly ash was encased by these hydration products, and the same phenomenon was also found in the literature [76]; these hydrates were attributed to the pozzolanic reaction of FA and NS. As reported in the literature [66], in the C-FA-NS system, a coating on the surface of FA could be formed by pozzolanic reaction of NS and FA, and it would possibly slow down the pozzolanic reaction of FA if the coating was better formed. Probably, this was one reason why NS reduced the strength of C-FA at the age of 90 d. In comparison with Figure 12(b), fly ash was encased by more amount of hydrates in Figure 12(c), and this indicated that more amount

of hydrates on the surface of FA particles was produced in the C-FA system with 4.0% NS. It was deduced that NS would significantly improve the interface between FA particles and cement particles, and this could contribute to compressive strength and impermeability.

Based on the discussion above, it was concluded that NS accelerated cement hydration, and most likely, it slightly hastened the pozzolanic reaction of FA. The amount of CH in hydrates was reduced due to the consumption of pozzolanic reaction of FA and NS; the amount of C-S-H gel was increased because of the accelerated hydration of cement and pozzolanic reaction of NS.

3.5. Mechanism. In the C-FA system, NS was able to significantly increase the impermeability, and the reason was revealed as follows: firstly, NS with nanosize could exert the filling effect to block capillary pore. Because of high reaction activity, it could efficiently take part in pozzolanic reaction and also act as nucleation seed to induce the cement hydration; accordingly, the formation of C-S-H gel with nanosize was facilitated, which could also fill or block the capillary pores greatly to improve the impermeability
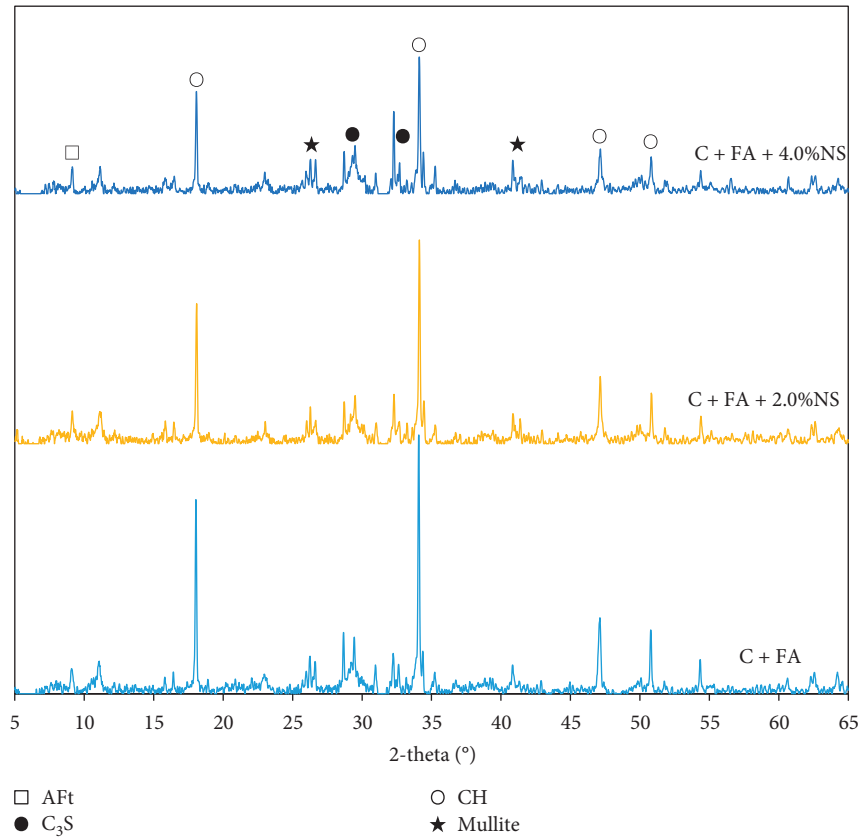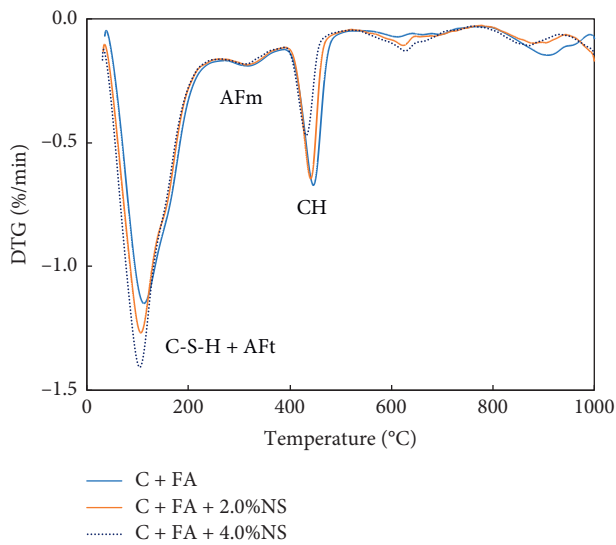
FIGURE 9: XRD patterns of hydrates.

FIGURE 10: DTG analysis of paste hydrated for 28 d.

TABLE 5: Weight loss of paste hydrated for 28 d.

Sample	Weight loss (%)		CH content (%)
	50–200°C	400–500°C	
C-FA	7.46	3.21	7.85
C-FA with 2.0% NS	8.29	2.67	6.53
C-FA with 4.0% NS	9.05	2.04	4.99
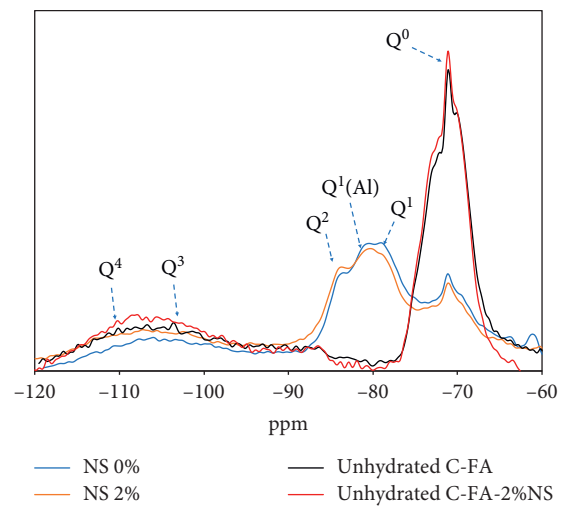
FIGURE 11: ^{29}Si-NMR pattern of paste hydrated for 28 d.

[77, 78]. Furthermore, NS induced the hydration of cement by consuming CH and acting as nucleation seed, and the hydration degree of the system was promoted. This significantly improved the microstructure, such as microstructure of C-S-H gel as well as the interface between FA and C-S-H gel, thereby enhancing impermeability. The pore structure

TABLE 6: Deconvolution results of the paste samples hydrated at 28d.

	Unhydrated C + FA	Unhydrated C + FA + 2% NS	C-FA	C-FA + NS 2%
Q^0 (%)	68.01	66.97	28.10	23.50
Q^1 (%)	—	—	25.90	26.50
Q^2 (%)	—	—	13.10	17.25
Q^2(1Al) (%)	—	—	8.02	9.70
$Q^3 + Q^4$ (%)	31.99	33.03	28.78	28.15
A_C (%)	—	—	58.68	64.91
A_{FA} (%)	—	—	10.03	—
A_{FA+NS} (%)	—	—	—	14.77
MCL	—	—	3.94	4.40
Al/Si (%)	—	—	0.085	0.091

(a)

(b)

(c)
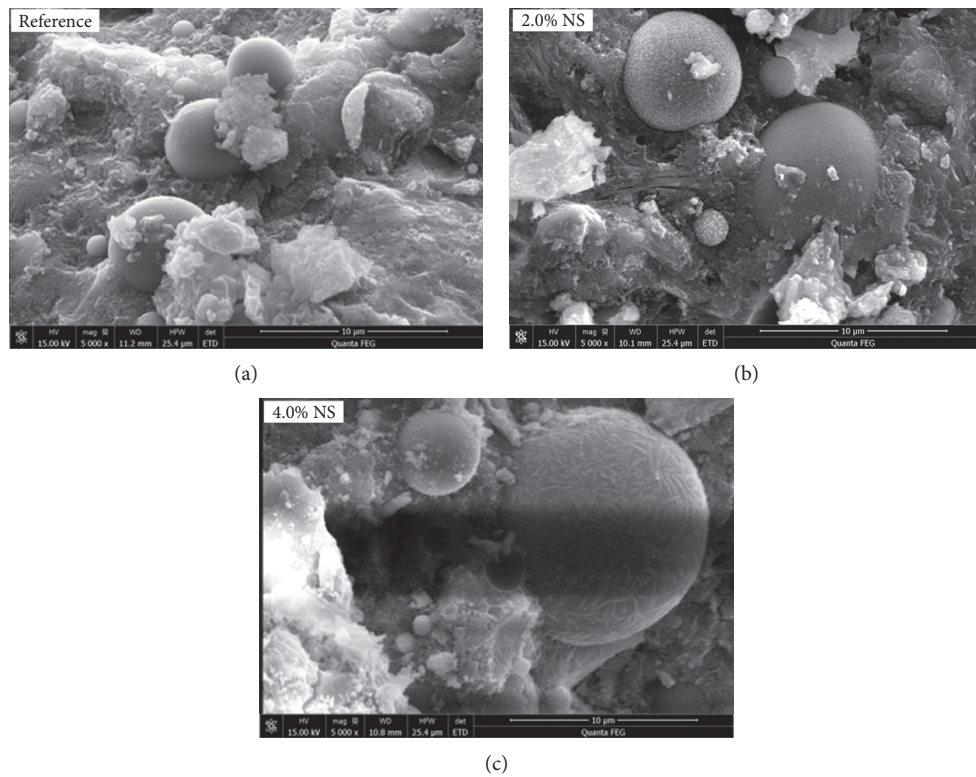
FIGURE 12: SEM images of C-FA hydrated for 28 d.

(a)

(b)

- Cement particle
- Hydration products
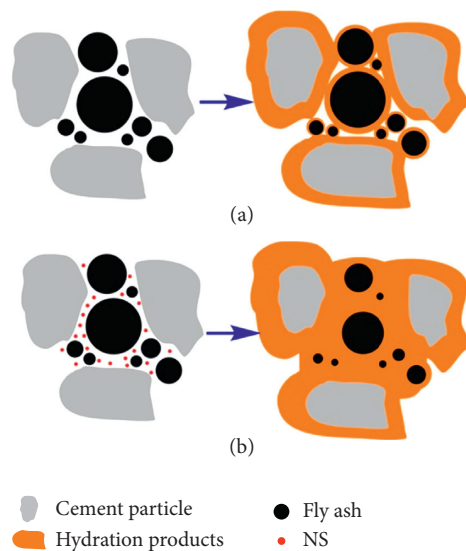- Fly ash
- NS

FIGURE 13: Mechanism behind the improvement in impermeability with NS. (a) C-FA. (b) C-FA with NS.

was refined and the microstructure was improved, with great contribution to the impermeability, as shown in Figure 13.

4. Conclusion

(1) In the C-FA-NS system, NS obviously refined the pore structure, increased the complexity of the pore structure, and improved the microstructure, and the reason was not only due to the filling effect of NS but also because of a large amount of hydrates formed to improve the microstructure.

(2) NS accelerated the whole hydration of the cement-FA system. NS not only consumed calcium hydroxide by the pozzolanic reaction to induce the cement hydration but also acted as nucleation seed to induce the formation of C-S-H gel, thereby accelerating the cement hydration. Probably, it also slightly accelerated the pozzolanic reaction of FA.

(3) NS significantly improved the impermeability of the cement-FA system, and this kind of materials would be expected to be used as surface protection material. However, the interface performance between SPM and matrix, such as shrinkage and bond strength, and how to cast SPM onto the surface of the matrix should be carefully considered.

Data Availability

The data used to support the findings of this study are available from the corresponding author upon request.

Conflicts of Interest

The authors declared that there were no conflicts of interest regarding the publication of this paper.

Acknowledgments

References

[1] Z. Zhang, Q. Wang, and H. Chen, "Properties of high-volume limestone powder concrete under standard curing and steam-curing conditions," *Powder Technology*, vol. 301, pp. 16–25, 2016.

[2] T. Liu, H. Wei, D. Zou, A. Zhou, and H. Jian, "Utilization of waste cathode ray tube funnel glass for ultra-high performance concrete," *Journal of Cleaner Production*, vol. 249, Article ID 119333, 2020.

[3] J. Zuquan, S. Wei, Z. Yunsheng, J. Jinyang, and L. Jianzhong, "Interaction between sulfate and chloride solution attack of concretes with and without fly ash," *Cement and Concrete Research*, vol. 37, no. 8, pp. 1223–1232, 2007.

[4] P. Zhang, F. H. Wittmann, P. Lura, H. S. Müller, S. Han, and T. Zhao, "Application of neutron imaging to investigate fundamental aspects of durability of cement-based materials:

[5] W. Jiang, X. Li, Y. Lv et al., "Cement-based materials containing graphene oxide and polyvinyl alcohol fiber: mechanical properties, durability, and microstructure," *Nanomaterials*, vol. 8, no. 9, p. 638, 2018.

[6] Y. Su, X. Wei, J. Huang et al., "Use of different barium salts to inhibit the thaumasite form of sulfate attack in cement-based materials," *Journal of Wuhan University of Technology-Mater. Sci. Ed.* vol. 31, no. 2, pp. 361–366, 2016.

[7] S. Uthaman, V. Vishwakarma, R. P. George et al., "Enhancement of strength and durability of fly ash concrete in seawater environments: synergistic effect of nanoparticles," *Construction and Building Materials*, vol. 187, pp. 448–459, 2018.

[8] F. U. A. Shaikh and S. W. M. Supit, "Chloride induced corrosion durability of high volume fly ash concretes containing nano particles," *Construction and Building Materials*, vol. 99, pp. 208–225, 2015.

[9] Y. Liu, Z. Qin, and B. Chen, "Experimental research on magnesium phosphate cements modified by red mud," *Construction and Building Materials*, vol. 231, Article ID 117131, 2020.

[10] R. Ragoug, O. O. Metalssi, F. Barberon et al., "Durability of cement pastes exposed to external sulfate attack and leaching: physical and chemical aspects," *Cement and Concrete Research*, vol. 116, pp. 134–145, 2019.

[11] Y. Deng, C. Zhang, and X. Wei, "Influence of lithium sulfate addition on the properties of Portland cement paste," *Construction and Building Materials*, vol. 50, pp. 457–462, 2014.

[12] B. Ma, T. Zhang, H. Tan et al., "Effect of TIPA on chloride immobilization in cement-fly ash paste," *Advances in Materials Science and Engineering*, vol. 2018, Article ID 4179421, 11 pages, 2018.

[13] B. Ma, X. Liu, H. Tan et al., "Utilization of pretreated fly ash to enhance the chloride binding capacity of cement-based material," *Construction and Building Materials*, vol. 175, pp. 726–734, 2018.

[14] X. Pan, Z. Shi, C. Shi, T.-C. Ling, and N. Li, "A review on concrete surface treatment part I: types and mechanisms," *Construction and Building Materials*, vol. 132, pp. 578–590, 2017.

[15] X. Pan, Z. Shi, C. Shi, T.-C. Ling, and N. Li, "A review on surface treatment for concrete—part 2: performance," *Construction and Building Materials*, vol. 133, pp. 81–90, 2017.

[16] C. Christodoulou, C. I. Goodier, S. A. Austin, J. Webb, and G. K. Glass, "Long-term performance of surface impregnation of reinforced concrete structures with silane," *Construction and Building Materials*, vol. 48, pp. 708–716, 2013.

[17] B. Pigino, A. Leemann, E. Franzoni, and P. Lura, "Ethyl silicate for surface treatment of concrete—part II: characteristics and performance," *Cement and Concrete Composites*, vol. 34, no. 3, pp. 313–321, 2012.

[18] F. Sandrolini, E. Franzoni, and B. Pigino, "Ethyl silicate for surface treatment of concrete—part I: pozzolanic effect of ethyl silicate," *Cement and Concrete Composites*, vol. 34, no. 3, pp. 306–312, 2012.

[19] Q. Xu, S. Zhan, B. Xu, H. Yang, X. Qian, and X. Ding, "Effect of isobutyl-triethoxy-silane penetrative protective agent on the carbonation resistance of concrete," *Journal of Wuhan University of Technology-Mater. Sci. Ed.* vol. 31, no. 1, pp. 139–145, 2016.

[20] R. Li, P. Hou, N. Xie, Z. Ye, X. Cheng, and S. P. Shah, "Design of SiO$_2$/PMHS hybrid nanocomposite for surface treatment of

cement-based materials," *Cement and Concrete Composites*, vol. 87, pp. 89–97, 2018.

[21] M. H. F. Medeiros and P. Helene, "Surface treatment of reinforced concrete in marine environment: influence on chloride diffusion coefficient and capillary water absorption," *Construction and Building Materials*, vol. 23, no. 3, pp. 1476–1484, 2009.

[22] B. Zhang, H. Tan, W. Shen, G. Xu, B. Ma, and X. Ji, "Nano-silica and silica fume modified cement mortar used as surface protection material to enhance the impermeability," *Cement and Concrete Composites*, vol. 92, pp. 7–17, 2018.

[23] J. Mei, B. Ma, H. Tan et al., "Influence of steam curing and nano silica on hydration and microstructure characteristics of high volume fly ash cement system," *Construction and Building Materials*, vol. 171, pp. 83–95, 2018.

[24] J. Mei, H. Tan, H. Li et al., "Effect of sodium sulfate and nano-SiO$_2$ on hydration and microstructure of cementitious materials containing high volume fly ash under steam curing," *Construction and Building Materials*, vol. 163, pp. 812–825, 2018.

[25] X. Yang, J. Liu, H. Li, L. Xu, Q. Ren, and L. Li, "Effect of triethanolamine hydrochloride on the performance of cement paste," *Construction and Building Materials*, vol. 200, pp. 218–225, 2019.

[26] T. Shi, Z. Li, J. Guo, H. Gong, and C. Gu, "Research progress on CNTs/CNFs-modified cement-based composites—a review," *Construction and Building Materials*, vol. 202, pp. 290–307, 2019.

[27] G. Li, B. Yang, C. Guo, J. Du, and X. Wu, "Time dependence and service life prediction of chloride resistance of concrete coatings," *Construction and Building Materials*, vol. 83, pp. 19–25, 2015.

[28] S. Sadati, M. Arezoumandi, and M. Shekarchi, "Long-term performance of concrete surface coatings in soil exposure of marine environments," *Construction and Building Materials*, vol. 94, pp. 656–663, 2015.

[29] Y. Wang, X. He, Y. Su, J. Yang, B. Strnadel, and X. Wang, "Efficiency of wet-grinding on the mechano-chemical activation of granulated blast furnace slag (GBFS)," *Construction and Building Materials*, vol. 199, pp. 185–193, 2019.

[30] K. Gu and B. Chen, "Loess stabilization using cement, waste phosphogypsum, fly ash and quicklime for self-compacting rammed earth construction," *Construction and Building Materials*, vol. 231, Article ID 117195, 2020.

[31] Q. Li, L. Zhang, X. Gao, and J. Zhang, "Effect of pulverized fuel ash, ground granulated blast-furnace slag and CO$_2$ curing on performance of magnesium oxysulfate cement," *Construction and Building Materials*, vol. 230, Article ID 116990, 2020.

[32] X. He, M. Ma, Y. Su et al., "The effect of ultrahigh volume ultrafine blast furnace slag on the properties of cement pastes," *Construction and Building Materials*, vol. 189, pp. 438–447, 2018.

[33] X. He, Q. Ye, J. Yang et al., "Physico-chemical characteristics of wet-milled ultrafine-granulated phosphorus slag as a supplementary cementitious material," *Journal of Wuhan University of Technology-Mater. Sci. Ed.* vol. 33, no. 3, pp. 625–633, 2018.

[34] F. Lavergne, R. Belhadi, J. Carriat, and A. Ben Fraj, "Effect of nano-silica particles on the hydration, the rheology and the strength development of a blended cement paste," *Cement and Concrete Composites*, vol. 95, pp. 42–55, 2019.

[35] F. Zou, H. Tan, Y. Guo, B. Ma, X. He, and Y. Zhou, "Effect of sodium gluconate on dispersion of polycarboxylate super-plasticizer with different grafting density in side chain," *Journal of Industrial and Engineering Chemistry*, vol. 55, pp. 91–100, 2017.

[36] X. Liu, B. Ma, H. Tan et al., "Effect of aluminum sulfate on the hydration of Portland cement, tricalcium silicate and tricalcium aluminate," *Construction and Building Materials*, vol. 232, Article ID 117179, 2020.

[37] H. Tan, M. Li, X. He et al., "Preparation for micro-lithium slag via wet grinding and its application as accelerator in Portland cement," *Journal of Cleaner Production*, vol. 250, Article ID 119528, 2020.

[38] B. Ma, T. Zhang, H. Tan et al., "Effect of triisopropanolamine on compressive strength and hydration of cement-fly ash paste," *Construction and Building Materials*, vol. 179, pp. 89–99, 2018.

[39] L. Qin and X. Gao, "Properties of coal gangue-Portland cement mixture with carbonation," *Fuel*, vol. 245, pp. 1–12, 2019.

[40] S. Bae, R. Taylor, D. Kilcoyne, J. Moon, and P. Monteiro, "Effects of incorporating high-volume fly ash into tricalcium silicate on the degree of silicate polymerization and aluminum substitution for silicon in calcium silicate hydrate," *Materials*, vol. 10, no. 2, p. 131, 2017.

[41] M. M. Al-Zahrani, A.-H. J. Al-Tayyib, S. U. Al-Dulaijan, and E. Osei-Twum, "29Si MAS-NMR study of hydrated cement paste and mortar with varying content of fly ash," *Advances in Cement Research*, vol. 18, no. 1, pp. 27–34, 2006.

[42] L. Zhang and B. Chen, "Hydration and properties of slag cement activated by alkali and sulfate," *Journal of Materials in Civil Engineering*, vol. 29, no. 9, 2017.

[43] S. C. Paul, A. S. Van Rooyen, G. P. A. G. Van Zijl, and L. F. Petrik, "Properties of cement-based composites using nanoparticles: a comprehensive review," *Construction and Building Materials*, vol. 189, pp. 1019–1034, 2018.

[44] B. Zhang and S. Li, "Determination of the surface fractal dimension for porous media by mercury porosimetry," *Industrial & Engineering Chemistry Research*, vol. 34, no. 4, pp. 1383–1386, 1995.

[45] J. Yang, Y. Su, X. He et al., "Pore structure evaluation of cementing composites blended with coal by-products: calcined coal gangue and coal fly ash," *Fuel Processing Technology*, vol. 181, pp. 75–90, 2018.

[46] Q. Zeng, K. Li, T. Fen-Chong, and P. Dangla, "Surface fractal analysis of pore structure of high-volume fly-ash cement pastes," *Applied Surface Science*, vol. 257, no. 3, pp. 762–768, 2010.

[47] B. Zhang, W. Liu, and X. Liu, "Scale-dependent nature of the surface fractal dimension for bi-and multi-disperse porous solids by mercury porosimetry," *Applied Surface Science*, vol. 253, no. 3, pp. 1349–1355, 2006.

[48] J. Yang, F. Wang, X. He, and Y. Su, "Pore structure of affected zone around saturated and large superabsorbent polymers in cement paste," *Cement and Concrete Composites*, vol. 97, pp. 54–67, 2019.

[49] M. Liu, H. Tan, and X. He, "Effects of nano-SiO$_2$ on early strength and microstructure of steam-cured high volume fly ash cement system," *Construction and Building Materials*, vol. 194, pp. 350–359, 2019.

[50] X. Gao, J. Zhang, and Y. Su, "Influence of vibration-induced segregation on mechanical property and chloride ion permeability of concrete with variable rheological performance," *Construction and Building Materials*, vol. 194, pp. 32–41, 2019.

[51] R. Zhang and D. K. Panesar, "Water absorption of carbonated reactive MgO concrete and its correlation with the pore

structure," *Journal of CO₂ Utilization*, vol. 24, pp. 350–360, 2018.

[52] D. Zou, K. Li, W. Li, H. Li, and T. Cao, "Effects of pore structure and water absorption on internal curing efficiency of porous aggregates," *Construction and Building Materials*, vol. 163, pp. 949–959, 2018.

[53] G. Quercia, P. Spiesz, G. Hüsken, and H. J. H. Brouwers, "SCC modification by use of amorphous nano-silica," *Cement and Concrete Composites*, vol. 45, pp. 69–81, 2014.

[54] B. Ma, J. Wang, H. Tan et al., "Utilization of waste marble powder in cement-based materials by incorporating nano silica," *Construction and Building Materials*, vol. 211, pp. 139–149, 2019.

[55] H. Tan, X. Zhang, X. He et al., "Utilization of lithium slag by wet-grinding process to improve the early strength of sulphoaluminate cement paste," *Journal of Cleaner Production*, vol. 205, pp. 536–551, 2018.

[56] P. Scarfato, L. Di Maio, M. L. Fariello, P. Russo, and L. Incarnato, "Preparation and evaluation of polymer/clay nanocomposite surface treatments for concrete durability enhancement," *Cement and Concrete Composites*, vol. 34, no. 3, pp. 297–305, 2012.

[57] F. Pittella, M. Zhang, Y. Lee et al., "Enhanced endosomal escape of siRNA-incorporating hybrid nanoparticles from calcium phosphate and PEG-block charge-conversional polymer for efficient gene knockdown with negligible cytotoxicity," *Biomaterials*, vol. 32, no. 11, pp. 3106–3114, 2011.

[58] B. Pang, Y. Zhang, G. Liu, and W. She, "Interface properties of nanosilica-modified waterborne epoxy cement repairing system," *ACS Applied Materials & Interfaces*, vol. 10, no. 25, pp. 21696–21711, 2018.

[59] G. Li, "Properties of high-volume fly ash concrete incorporating nano-SiO₂," *Cement and Concrete Research*, vol. 34, no. 6, pp. 1043–1049, 2004.

[60] D. Kong, D. J. Corr, P. Hou, Y. Yang, and S. P. Shah, "Influence of colloidal silica sol on fresh properties of cement paste as compared to nano-silica powder with agglomerates in micron-scale," *Cement and Concrete Composites*, vol. 63, pp. 30–41, 2015.

[61] P. Zhang, J. Wan, K. Wang, and Q. Li, "Influence of nano-SiO₂ on properties of fresh and hardened high performance concrete: a state-of-the-art review," *Construction and Building Materials*, vol. 148, pp. 648–658, 2017.

[62] Y. Wang, X. He, Y. Su et al., "Self-hydration characteristics of ground granulated blast-furnace slag (GGBFS) by wet-grinding treatment," *Construction and Building Materials*, vol. 167, pp. 96–105, 2018.

[63] J. Yang, J. Huang, X. He et al., "Segmented fractal pore structure covering nano-and micro-ranges in cementing composites produced with GGBS," *Construction and Building Materials*, vol. 225, pp. 1170–1182, 2019.

[64] Y. Jeong, W. S. Yum, D. Jeon, and J. E. Oh, "Strength development and microstructural characteristics of barium hydroxide-activated ground granulated blast furnace slag," *Cement and Concrete Composites*, vol. 79, pp. 34–44, 2017.

[65] Q. Wang, D. Wang, and H. Chen, "The role of fly ash microsphere in the microstructure and macroscopic properties of high-strength concrete," *Cement and Concrete Composites*, vol. 83, pp. 125–137, 2017.

[66] P. Hou, K. Wang, J. Qian, S. Kawashima, D. Kong, and S. P. Shah, "Effects of colloidal nano SiO₂ on fly ash hydration," *Cement and Concrete Composites*, vol. 34, no. 10, pp. 1095–1103, 2012.

[67] M. Rupasinghe, R. San Nicolas, P. Mendis, M. Sofi, and T. Ngo, "Investigation of strength and hydration characteristics in nano-silica incorporated cement paste," *Cement and Concrete Composites*, vol. 80, pp. 17–30, 2017.

[68] X. Yang, J. Liu, H. Li, and Q. Ren, "Performance and ITZ of pervious concrete modified by vinyl acetate and ethylene copolymer dispersible powder," *Construction and Building Materials*, vol. 235, Article ID 117532, 2020.

[69] H. Li, C. Xu, B. Dong et al., "Differences between their influences of TEA and TEA·HCl on the properties of cement paste," *Construction and Building Materials*, vol. 239, Article ID 117797, 2020.

[70] Y. Qing, Z. Zenan, K. Deyu, and C. Rongshen, "Influence of nano-SiO₂ addition on properties of hardened cement paste as compared with silica fume," *Construction and Building Materials*, vol. 21, no. 3, pp. 539–545, 2007.

[71] C. Xu, H. Li, and X. Yang, "Effect and characterization of the nucleation C-S-H seed on the reactivity of granulated blast furnace slag powder," *Construction and Building Materials*, vol. 238, Article ID 117726, 2020.

[72] L. Lang, N. Liu, and B. Chen, "Strength development of solidified dredged sludge containing humic acid with cement, lime and nano-SiO₂," *Construction and Building Materials*, vol. 230, Article ID 116971, 2020.

[73] H. Tan, K. Nie, X. He et al., "Compressive strength and hydration of high-volume wet-grinded coal fly ash cementitious materials," *Construction and Building Materials*, vol. 206, pp. 248–260, 2019.

[74] J. Yang, J. Huang, Y. Su et al., "Eco-friendly treatment of low-calcium coal fly ash for high pozzolanic reactivity: a step towards waste utilization in sustainable building material," *Journal of Cleaner Production*, vol. 238, 2019.

[75] M. Wu, Y. Zhang, Y. Ji et al., "Reducing environmental impacts and carbon emissions: study of effects of superfine cement particles on blended cement containing high volume mineral admixtures," *Journal of Cleaner Production*, vol. 196, pp. 358–369, 2018.

[76] F. Moghaddam, V. Sirivivatnanon, and K. Vessalas, "The effect of fly ash fineness on heat of hydration, microstructure, flow and compressive strength of blended cement pastes," *Case Studies in Construction Materials*, vol. 10, Article ID e00218, 2019.

[77] H. Tan, X. Deng, X. He et al., "Compressive strength and hydration process of wet-grinded granulated blast-furnace slag activated by sodium sulfate and sodium carbonate," *Cement and Concrete Composites*, vol. 97, pp. 387–398, 2019.

[78] Y. Gu, Q. Ran, X. Shu, C. Yu, H. Chang, and J. Liu, "Synthesis of nanoSiO2@PCE core-shell nanoparticles and its effect on cement hydration at early age," *Construction and Building Materials*, vol. 114, pp. 673–680, 2016.